WS_2 thin films prepared by solid state reaction (induced by annealing) between the constituents in thin film form

1996 J. Phys.: Condens. Matter 8 2291

(http://iopscience.iop.org/0953-8984/8/14/006)

J. Phys.: Condens. Matter **8** (1996) 2291–2304. Printed in the UK

WS_2 thin films prepared by solid state reaction (induced by annealing) between the constituents in thin film form

S J Li, J C Bernède, J Pouzet and M Jamali

Université de Nantes, Laboratoire de Physique des Materiaux pour l'Electronique, Equipe Couches Minces et Materiaux Nouveaux, Faculté des Sciences et des Techniques, 2 rue de la Houssinière, 44072 Nantes Cédex 03, France

Received 21 July 1995, in final form 23 October 1995

Abstract. WS_2 thin films were obtained by solid state reaction (induced by annealing under S pressure) between the W and S constituents in thin film form. The tungsten layers were deposited by RF sputtering, while S layers were evaporated. The thickness of the layers varied between 50 and 100 nm. The films have been investigated using x-ray photoelectron spectroscopy, scanning electron microscopy, x-ray diffraction, optical absorption and conductivity measurements. The effects of annealing conditions (duration and temperature) on the crystallization and composition of the films have been investigated. The films were crystallized in the 2H–WS_2 hexagonal structure. To complete the reaction between W and S, annealing under S pressure at a temperature of at least 820 K for 24 h is required. Under these conditions the films were nearly stoichiometric. The best films present a *c*-axis length of 1.2500 nm and an *a*-axis length of 0.3185 nm. All the films were found to be preferentially oriented with the *c* axis perpendicular to the plane of the substrate. The degree of preferential orientation was found to increase slightly with increasing annealing time and/or temperature. The nearly stoichiometric films present good optical properties, similar to those of single crystals. The conductivity of the films depends strongly on the annealing conditions, i.e. on their composition and on their crystallization state.

1. Introduction

Layered-structure transition metal dichalcogenides MX_2 (M = W or Mo; X = Se or S) have been extensively investigated. Some investigations were mainly related to the lubricating properties of MS_2 [1–4], and others to the photovoltaic properties of MSe_2 [5–11]. However, the resource abundance and the non-toxicity of sulphur have to be taken into account for applications. Since the band gap of WS_2 is well matched to the solar spectrum [12], it can act as an efficient photoconductive layer in a photovoltaic device. Moreover it can be used as electrodes in the realization of photoelectrochemical solar cells. The main advantage of WS_2 is the prevention of electrolyte corrosion, because the phototransitions involve non-bonding d–d orbitals of W atoms [5]. Pawlikowski [13] has shown that the performance of photoelectric devices may be improved by growing thin films that have vertical grain boundaries; so it should be interesting to obtain textured WS_2 thin films. Therefore we have investigated a new technique to obtain WS_2 thin films. Many methods have been used to produce WS_2 thin films: MOCVD [14, 15], vapour transport [16], pulsed-laser deposition [17], molecular beam epitaxy [18] and sulphurization of sputtered tungsten films using H_2S [19, 20] or in a closed-tube system using sulphur [12].

In the laboratory a very cheap and simple technique called solid state reaction between the constituents in thin film form has been used to obtain stoichiometric textured WSe_2

0953-8984/96/142291+14$19.50

films [21, 22]. In this paper we report the first results obtained with this technique for the realization of WS_2 layers.

2. Experiments

2.1. Preparation

The WS_2 thin films were prepared analogously to the WSe_2 films obtained by solid state reaction (induced by annealing) between the constituents in thin film form [21]. The substrates were polished glass, chemically cleaned.

For the S and W deposition process, the films were deposited in vacuum (base pressure, 5×10^{-4} Pa) by evaporation of S and sputtering of W. Sulphur was deposited by classical thermal evaporation from a tantalum crucible, while W was deposited by RF sputtering using a diode system. The evaporation rates and film thicknesses were measured *in situ* by the vibrating-quartz method. The W films were sputtered from a tungsten target foil (diameter, 75 mm; thickness, 0.25 mm). The sputtering argon pressure was 5 Pa, the target–substrate distance was 1.5 cm and the sputtering power was 100 W. Prior to the first sputter deposition the target was cleaned by pre-sputtering; then the shutter was removed and the deposition started. The purity of S was 99.999% and that of W was 99.99%. The WS_2 films were synthesized by solid state reaction (induced by annealing) between the W and S films.

Layers of W and S were deposited sequentially. During the deposition the rotating substrate holder was successively positioned in front of the S evaporation source and in front of the W target according to the sequence. The number of layers varied from six to ten in order to deposit W/S/W/ . . . /W/S structures. After deposition the multilayer structures were annealed. Therefore, since sulphur has a high vapour pressure while tungsten does not, during the anneal the last sulphur layer was evaporated and the thicknesses of the other layers were calculated to achieve the desired composition, varying from 25 to 50 nm and from 90 to 175 nm for W and S, respectively.

After deposition, the samples were annealed in a vacuum-sealed glass tube. Thus the last amorphous sulphur capping layer not only protects the tungsten films from oxidation during transfer from the deposition apparatus to the glass tube but also permits us to carry out the anneal under a small sulphur pressure, which increases the quality of the films as shown in the case of WSe_2 [21]. The annealing temperature varies from 770 to 870 K while the duration varies from 2 to 24 h. Details of typical samples studied are given in table 1. As shown for selenium in the case of WSe_2 [21], during the cooling of the glass tube, some sulphur condensation takes place on the surface of the films (table 2). This sulphur excess is sublimated by annealing the samples under dynamic vacuum for 4 h at $T = 670$ K.

2.2. Thin film characterization

The total thickness of the films was measured with a mechanical stylus profilmeter. This method requires the presence of a step between the substrate surface and the film surface so that the stylus is vertically displaced as it traverses the sample. Such steps can be produced by masking portions of the substrate during depositions. Masking requires that the mask is in close contact with the substrate and is very thin in order to avoid shadowing and accumulation of material near the step edge. Therefore a cover glass was used as a mask.

The thin film composition was obtained from x-ray photoelectron spectroscopy (XPS)

Table 1. Typical samples studied in this paper.

Typical samples studied	Number of sequentially deposited layers	Total thickness (nm)	Annealing under sulphur atmosphere		Annealing under dynamic vacuum	
			Temperature (K)	Time (h)	Temperature (K)	Time (h)
VJC2	14	100	820	24	670	4
VJC3	14	100	870	2	670	4
VJC6	10	-60	820	24	670	4
VJC35	14	100	770	24	670	4

Table 2. XPS analyses and microprobe analyses.

Sample	Binding energy (eV)			Composition (at.%)	
	S 2p	W $4f_{5/2}$	W $4f_{7/2}$	W	S
S [21]	164.05				
W [21]		33.15	31		
WS_2 [21]	161.9	33.65	31.6	33.33	66.67
Thin film annealed at $T = 820$ K for 24 h not post-annealed under a dynamic vacuum				<30	>70
Thin film annealed under sulphur atmosphere at $T = 870$ K for $t = 2$ h VJC3	162	33.15	32	36 (34[a])	64 (66[a])
The above film post-annealed under a dynamic vacuum $T = 670$ K; $t = 4$ h (film thickness, 100 nm) VJC3	162	33.15	32	32 (33[a])	68 (67[a])
$T = 820$ K, $t = 24$ h (film thickness, 100 nm)				(35[a])	(65[a])

[a] Microprobe analyses.

measurements and microprobe analysis. The XPS apparatus and experimental conditions have been described previously [11]. XPS analysis was carried out at the University of Nantes, CNRS, on a Leybold HS-12 spectrometer. XPS measurements were performed with a magnesium x-ray source (1253 eV) operating at 10 kV and 10 mA. Data acquisition and treatment are realized through a computer and a standard program. The quantitative studies were based on the determination of the W 4f and S 2p peak areas of 2.14 and 0.44, respectively, as sensitivity factors (the sensitivity factors of the spectrometer are given by the manufacturer Leybold).

Detailed morphological analysis of the films was carried out by scanning electron microscopy (SEM) using a JEOL 6400F field emission electron microscope. Another electron microscope equipped with a microprobe analyser was used to check the composition of the films.

An x-ray diffractometer using monochromatic Cu Kα radiation was employed to obtain diffraction patterns from the films. The relative intensities of the diffraction patterns were

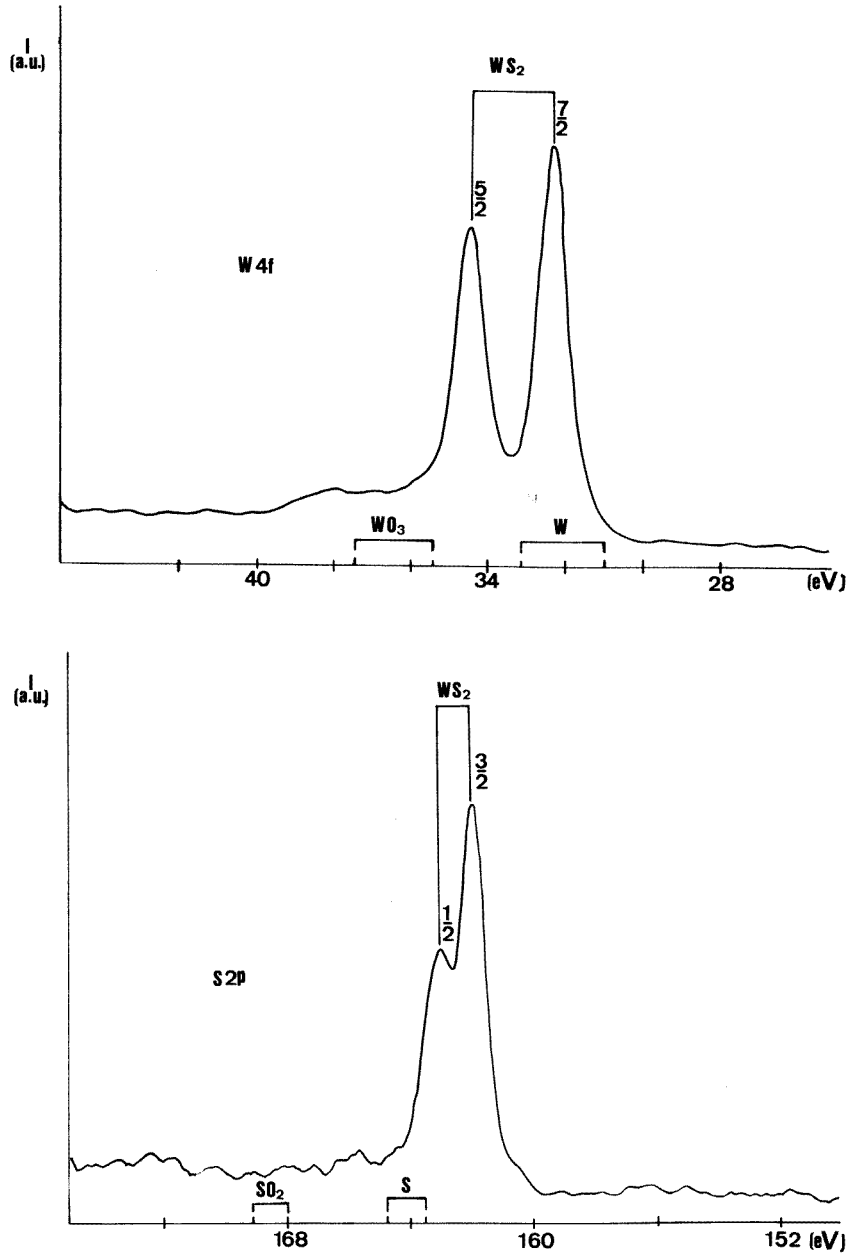

Figure 1. X-ray photoelectron spectrum of a WS_2 film: (a) W 4f; (b) S 2p; (c) O 1s.

used to determine the presence of preferred crystallographic orientations [23]. Optical measurements were carried out at room temperature and liquid-nitrogen temperature using a Cary 2300 spectrophotometer. The optical density was measured between 400 and 2000 nm.

For electrical measurements, gold electrodes were evaporated after the synthesis of the WS_2 thin films. The films are p-type semiconductors as shown by the hot-probe technique.

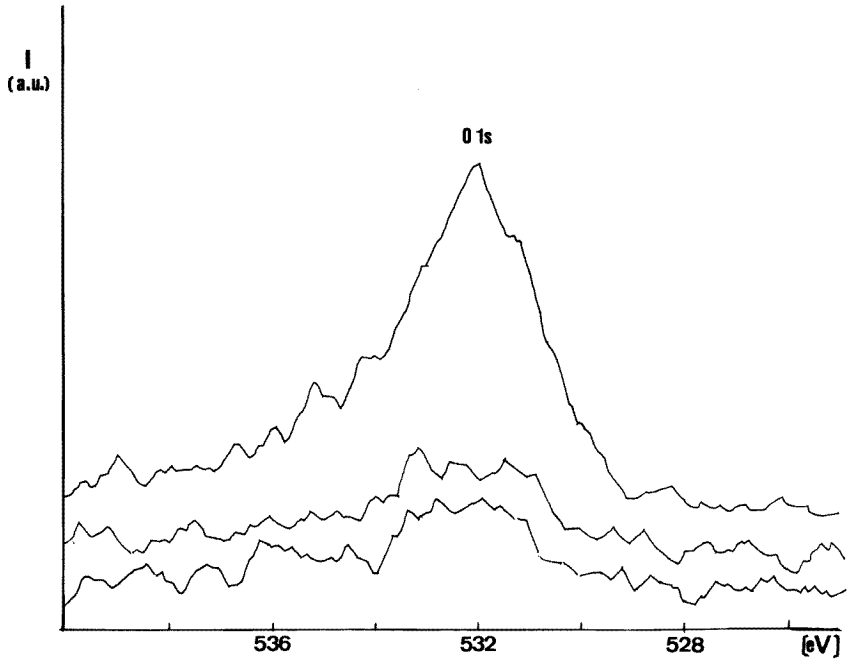

Figure 1. (Continued)

The DC conductance of the films was measured between 80 and 500 K by conventional methods (two wires) with an electrometer. The electrometer used was a Keithley model 617. In the ohms function, the currents generated during measurement were between 1 nA (2 MΩ < R < 2 GΩ) and 100 μA (2 kΩ < R < 20 kΩ). Electrical measurements were carried out in the dark. Gold gives a good ohmic contact.

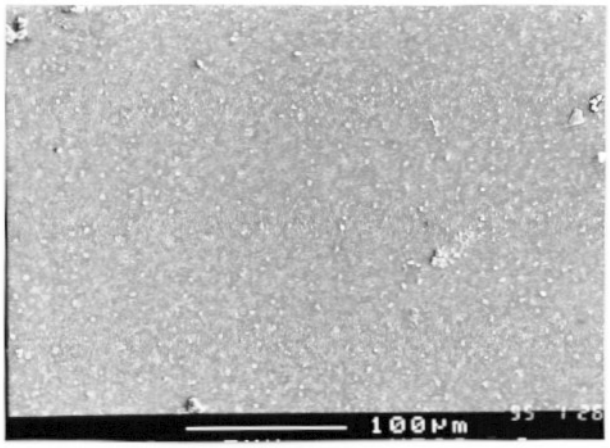

Figure 2. Microphotograph of a WS_2 film (low magnification).

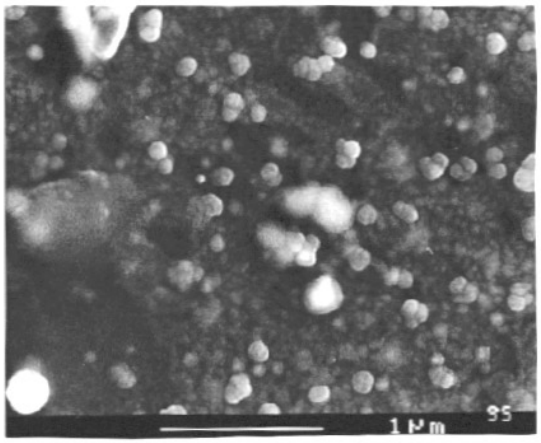

(*a*)

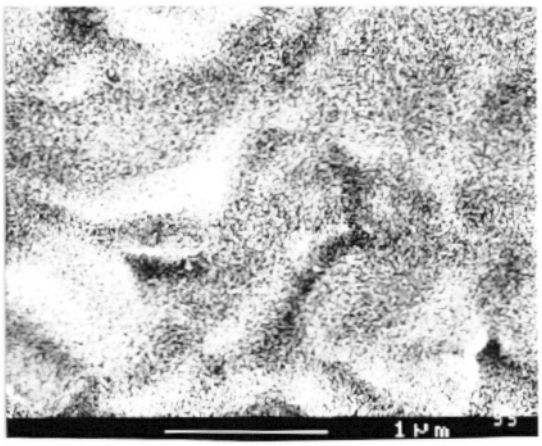

(*b*)

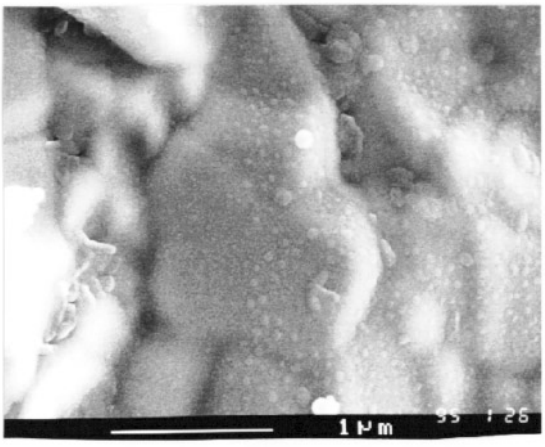

(*c*)

Figure 3. High-magnification microphotograph of WS_2 films after annealing: (a) $T = 820$ K, $t = 24$ *h*; (b) $T = 770$ K, $t = 24$ h; (c) $T = 870$ K, $t = 2$ h.

3. Results

3.1. Physicochemical and crystallographic characterization

The film thicknesses investigated in this work varied from 50 to 100 nm. At the end of the annealing process, all the samples exhibit nearly the same x-ray photoelectron spectrum (figure 1 and table 2). The binding energies are very close to those in [24]. The oxygen pollution of the layers is very small as can be seen after ion etching the atmospheric contamination at the surface of the film (figure 1(c)). After etching for 3 min the oxygen is not quantifiable, the W 4f and S 2p peaks are not represented because the etching speed of S is far higher than that of W and therefore the W–S bonds are destroyed, which modifies the shape and the binding energy of these peaks.

Quantitative analyses (table 2) show that the layers are nearly stoichiometric. The composition has been checked by microprobe analysis. However, as the films are very thin, the substrate is also detected by this technique. Moreover the silicon substrate peak overlaps the tungsten peak.

Therefore we have used a long acquisition time (500 s) and then we have used the curved-fitting programs included in the apparatus to discriminate between the two peaks. Typical 'net counts' measured by the apparatus are around $22\,000 \pm 200$ and 6000 ± 300 for S and W, respectively. The values obtained are not very different from those obtained by XPS (table 2). It can be concluded that the films are homogeneous and stoichiometric.

The surface of the films has been visualized by SEM. At a low magnification (figure 2) it can be seen that the surface of the films is homogeneous without large cracks or pinholes, which is quite different from the results obtained with some WSe_2 films [21, figure 4]. At a higher magnification (figure 3) it can be seen that the surface of the films is more or less rough. The shape of the crystallites depends on the annealing conditions. After an anneal at 820 K for 24 h (figure 3(a)) the grain size varies strongly from one crystallite to another (10–100 nm). These grains are randomly distributed in the film. For a lower temperature the grains are not well resolved (figure 3(b)) while for a shorter annealing time, if the grains are smaller (about 10 nm), the size of the crystallites does not vary strongly (figure 3(c)).

The x-ray diffraction spectra are reported in figure 4. Since the films are very thin the maximum intensity of the x-ray diffraction peaks is not very high (1400 counts s^{-1} at most); however, it can be seen (figure 4 and table 3) that all the films are crystallized in the 2H-WS_2 hexagonal structure.

All the films are polycrystalline with a high preferential orientation.

Table 3. XRD analysis.

	Annealing conditions		$hk.l = 00.2$		$hk.l = 00.4$		$hk.l = 10.1$				
Sample	Thickness (nm)	Temperature (K)	Time (h)	$d_{00.2}$	Counts (s^{-1})	$d_{00.4}$	Counts (s^{-1})	$d_{10.1}$	Counts (s^{-1})	$F_{00.l}$	FWHM (d°)	$D_{00.2}$ (nm)
VJC2	100	823	24	6.184	1644	3.094	95	—	—	1	0.8658	9.2
VJC3	100	873	2	6.2	1400	3.1	45	2.694	95	0.82	1.2999	6.2
VJC6	60	823	24	6.235	737	—	—	—	—	1	1.2851	6.1
VJC354	100	773	24	6.223	268	—	—	2.689	91	0.42	0.9677	8.3

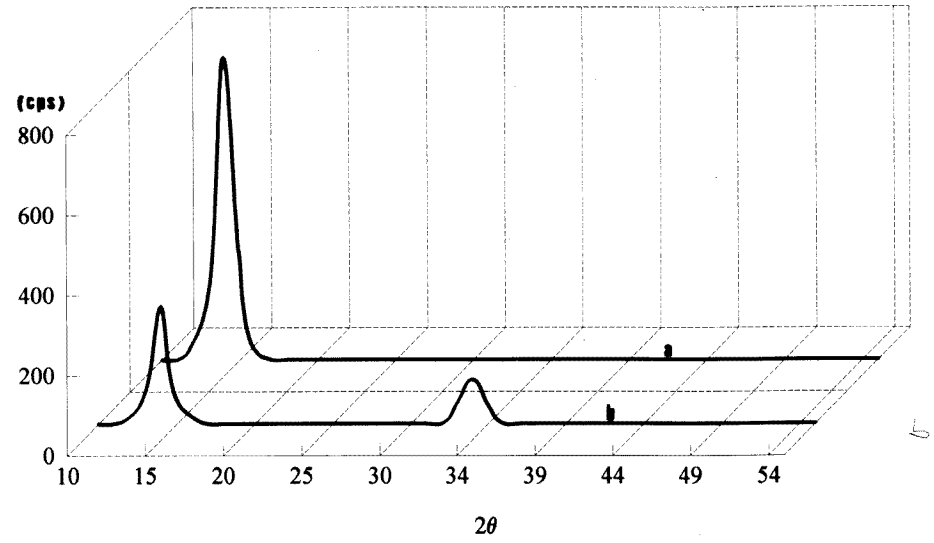

Figure 4. X-ray diffraction spectra of WS_2 films after annealing: (a) $T = 820$ K, $t = 24$ h; (b) $T = 770$ K, $t = 24$ h.

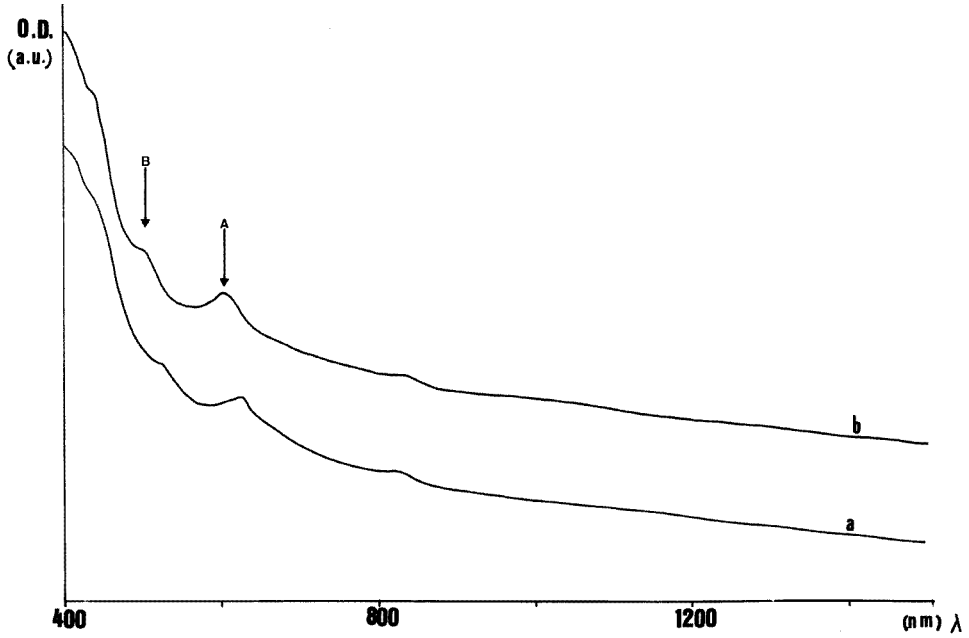

Figure 5. Variation in the optical absorption with photon energy: (a) at room temperature; (b) at liquid-nitrogen temperature.

3.2. Optical and electrical study

The optical measurements have been performed at liquid-nitrogen temperature and room temperature. A typical absorption curve obtained with films annealed for 24 h at 820 K is

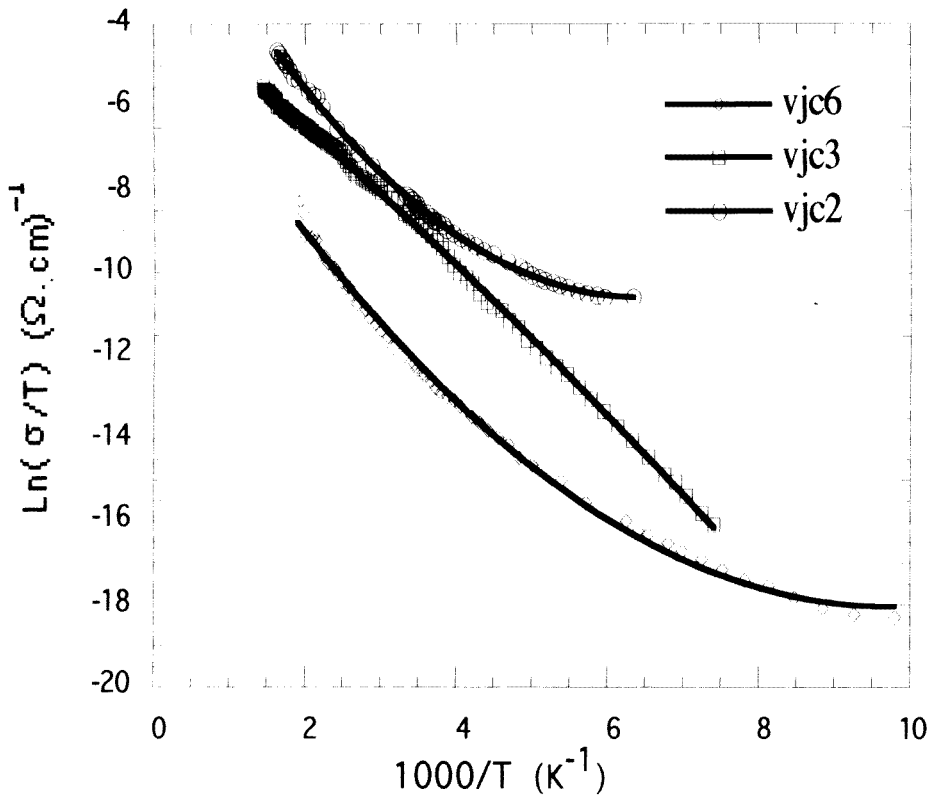

Figure 6. Typical temperature dependences of the theoretical resistance of WS_2 thin films.

Table 4. Characteristics of the fine structure in the spectra of WS_2 annealed for 24 h at 820 K.

Sample	Optical gap (eV)	Exciton peak A (eV)	Exciton peak B (eV)
Single crystal [26]			
$T = 300$ K	1.3		
$T = 77$ K		2.06	2.50
Thin film			
$T = 300$ K	1.3	2.0	2.386
$T = 77$ K	1.42	2.06	2.47

presented in figure 5. By comparison with the single crystal [26], the two main peaks A and B may be identified as due to excitons.

The temperature dependence of the electrical conductivity between 100 and 600 K is shown in figure 6. The room-temperature conductivity of the films is reported later in table 5.

4. Discussion

WS_2 thin films were synthesized by solid state reaction (induced by annealing) between the constituents in thin film form. XPS measurements (table 2) were found to be in good accordance with [24]. The films are nearly stoichiometric. They are crystallized in the 2H-WS_2 hexagonal structure.

The measured values of the interplanar spacing and the intensities in counts per second of the corresponding diffraction peaks are reported in table 3. The interplanar spacings are in good agreement with the data given in the *ASTM X-ray Powder Diffraction File* B 237. c and a determined from the expression calculated for hexagonal crystals [21] are 1.2368 ± 0.0005 nm and 0.3145 ± 0.0005 nm for the best films, which is in close agreement with the values reported in the ASTM data ($c = 1.2362$ nm; $a = 0.3157$ nm).

The degree $F_{00.l}$ of preferential orientation [25], that is to say the percentage of crystallites which have their c axis perpendicular to the plane of the substrate, is reported in table 3. It can be seen that the degree of texture of the films increases with increasing annealing temperature and/or annealing time.

The average grain size of the films estimated from the full width at half-maximum of the x-ray diffraction peak (00.2) is also reported in table 3. The size of the crystallites is quite small (10 nm or less).

The optical density measurements also show that the films are WS_2 films since their absorption spectra are in good agreement with that of the WS_2 single crystal.

Table 5. Physical parameters deduced from the plots of figure 6: homogeneity and quality factors.

		Annealing conditions							
Sample	Thickness (nm)	Temperature (K)	Time (h)	Bulk W concentration (at.%)	Room-temperature conductivity (Ω^{-1} cm^{-1})	$q\phi$ (meV)	σ_ϕ (mV)	$H = \phi/\sigma_\phi$	Q [32]
VJC2	100	823	24	39	9×10^{-2}	286	62	4.6	0.02
VJC3	100	873	2	39	5×10^{-2}	150	—	—	—
VJC6	60	823	24	32	2×10^{-3}	252	41	5.35	0.0006

The results are summarized in table 4. The absorption threshold in WS_2 gives rise to two strong absorption peaks labelled A and B. Peaks A and B are the first members of the two exciton series conventionally attributed to transitions from a spin–orbit split valence band.

The absorption coefficient α of WS_2 was calculated from the transmission spectra of two samples of different thicknesses as described by Bichsel and Levy [8]. The optical band gap of WS_2 films was estimated by extrapolating the straight lines of $\alpha^{1/2}$ versus $h\nu$, WS_2 being a layered indirect-band-gap semiconductor; the value of n is $1 \leqslant n \leqslant 2$ (table 4).

As expected, when the measurement temperature is decreased from room temperature to liquid-nitrogen temperature, the features of the transmission spectra are better resolved and the energies of these features are shifted towards higher values. However, since the films are deposited on a glass substrate, there could have been considerable tensile stress in them as the temperature was lowered, owing to the different expansion coefficients of the films and the substrate. The effect of this tension is primarily to shift any features in the spectra of the films compared with the unstrained crystals, and some broadening of these features is also inevitable [21]. This shift could be as much as 20 meV.

Therefore, it can be seen in table 4 that the measured energies in the present work

are in good agreement with those expected in WS_2. The increase in linewidth of the exciton features of the films may correspond not only to the effect of strains during cooling as discussed before but also to imperfections in the crystalline structure, the films being polycrystalline.

The structural characterization of the WS_2 films has shown that, if they are textured, their crystallites are very small. Therefore, in the planar configuration used for the electrical measurements, the grain boundaries will introduce a very important contribution in the conductivity process. This is corroborated by the room-temperature conductivity reported in table 5 which is one or two orders of magnitude smaller than that of WS_2 single crystals. Therefore the grain boundary theories have to be taken into account. The grain boundary trapping theory assumes the process of trapping states at the grain boundaries, which capture and therefore immobilize free carriers. These charged states at the grain boundaries create potential barriers which impede the passage of carriers from a grain to a neighbouring grain. This model explains most of the electrical properties of polycrystalline materials [27].

It is well known that, whatever the model used for the description of the thermoionic emission over the grain boundary, nearly a straight line should be obtained by plotting $\ln\sigma = f(1/T))$ the slope of the curve being related to the barrier height Φ_b by

$$\sigma \propto T^n \exp[-\phi_b/kT]$$

where k is the Boltzmann constant and n varies from one model to another: $n = -\frac{1}{2}$ [27], $n = +1$ [28], and $n = -\frac{1}{2}$ [29].

It can be seen in figure 6 that, in the temperature range studied, only the sample VJC3 is near to an Arrhenius dependence. For the other samples reported, the conductivity does not follow an Arrhenius dependence, which is often the case in polycrystalline films. Recently Werner [30] has shown that potential fluctuations at the grain boundaries result in curved conductivity plots for polycrystalline semiconductors, even if thermal carrier emission across the barrier is the only current transport process.

If we model the fluctuating barrier ϕ by a Gaussian distribution [31], then

$$P(\phi) = \frac{1}{\sigma_\phi\sqrt{2\pi}} \exp\left[-\frac{(\bar{\phi}-\phi)^2}{2\sigma_\phi^2}\right]$$

with $\bar{\phi}$ the mean barrier and σ_ϕ the standard deviation.

Werner has shown that the temperature-dependent activation energy E_{act} in figure 6 is given by

$$E_{act}(T) = -k\frac{\mathrm{d}}{\mathrm{d}T^{-1}}\left[\ln\left(\frac{\phi}{T}\right)\right] = q\left(\bar{\Phi}(T=0) - \frac{\sigma_\phi^2}{kT/q}\right).$$

The plots deduced from the derivatives of the curves of figure 6 are shown in figure 7. The corresponding values obtained for $\bar{\phi}$ and σ_ϕ are reported in table 5; such a calculation has not been done for VJC3 since it nearly follows the Arrhenius law.

The values obtained for ϕ and σ are in good agreement with preceding values obtained on other MX_2 layers synthesized by the same technique [32, 33]. Since the sample VJC3 does not need the Werner model, this means that this sample exhibits smaller barrier fluctuations, that is to say that it is more homogeneous than the other samples. However, its resistivity is not lower than those of other samples such as VJC2 which have the same composition.

Some similar results have been obtained on silicon thin films [34]. Fortin and co-workers have shown that the electrical properties of polycrystalline silicon films obtained by post annealing of amorphous silicon films deposited by VLPCVD depends on the annealing time.

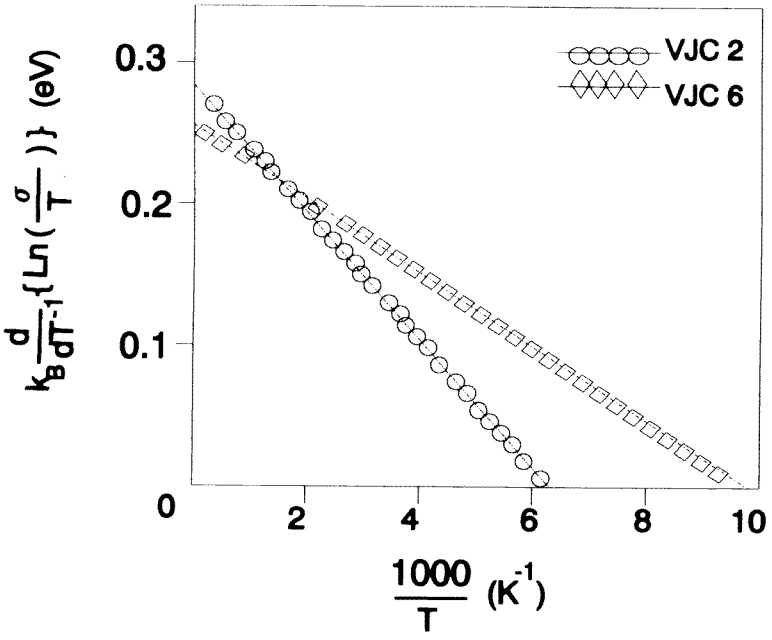

Figure 7. Slope of the curved plots in figure 6.

For short annealing times (3 h at 873 K), the polycrystalline films follow an Arrhenius plot $\ln\sigma = f(1/T)$ which corresponds to the classical thermionic emission model at the grain boundary. When the crystalline properties of the films are improved by a longer annealing time (12 h), the conductivity no longer follows an Arrhenius law and its variation with temperature is in good accordance with the Werner model.

Fortin and co-workers explain this evolution with the annealing time by the competition between the two processes.

(i) The quality of the crystallites is improved by annealing; impurities and defects migrate towards the grain boundaries where they accumulate,

(ii) The concentration of impurities and defects increases at the grain boundaries which induces barrier height inhomogeneities.

Therefore there is an optimum annealing time for improving the quality of the grains without strong degradation of the grain boundaries. In the present work this optimum is situated around the annealing conditions used for the VJC3 sample (table 1, 870 K for 2 h). This result is in good accordance with the SEM study (figure 3) which has shown that these films are well crystallized and that they are the more homogeneous.

5. Conclusion

In this work it has been shown that the technique called solid state reaction (induced by annealing) between the constituents in thin film form, used earlier to obtain $MoSe_2$ and WSe_2 films can also be used to obtain WS_2 films. This technique has the advantage that it is quite a cheap low-temperature process. Thin stoichiometric WS_2 films have been obtained by post annealing at 770 K $\leqslant T \leqslant$ 870 K for 2 h $\leqslant t \leqslant$ 24 h. The films are

crystallized in the 2H–WS_2 configuration. The degree of texture of the films increases with the annealing temperature and/or duration time. However, the crystallite size remains quite small ($D \leqslant 10$ nm). The optical properties of the films are in close accordance with those of the single crystal, which corroborates the good properties of the microcrystallites. The conductivity properties have been explained with the help of the fluctuating potential model introduced by Werner.

It is shown that the annealing time and temperature should be optimized in order to improve the quality of the grains without strong degradation of the grain boundary. We have shown earlier in the case of WSe_2 that the best electrical properties are not systematically obtained with the films which present the best crystallization properties (texture and grain size) [33]. Therefore a systematic study is under way in the laboratory to optimize structural and electrical properties of the films by varying the temperature and the duration of the annealing.

Acknowledgments

This work was supported by a contract between the EEC and the LPME (JOU II CT 930352). The authors wish to thank Mr Barreau for SEM measurements and Mr Fortin and Mr Brahim for helpful discussions. XPS analyses have been carried out at Nantes with a Leybold spectrometer (University of Nantes, CNRS).

References

[1] Dimigen H, Hubsch H, Willich P and Reichelt K 1979 *Thin Solid films* **64** 221
[2] Christy R J 1980 *Thin Solid Films* **73** 299
[3] Spalvins T 1982 *Thin Solid Films* **96** 17
[4] Fleischauer P D 1987 *Thin Solid Films* **154** 309
[5] Tributsch H 1979 *Solar Energy Mater.* **1** 257
[6] Kam K K and Parkinson B 1982 *J. Phys. Chem.* **86** 463
[7] Chandra S and Pandey R K 1982 *Phys. Status Solidi* a **72** 415
[8] Bichsel R and Levy F 1984 *Thin Solid Films* **116** 367; 1985 *Thin Solid Films* **124** 75
Bichsel R, Levy F and Mathieu 1985 *Thin Solid Films* **131** 87
[9] Jager-Waldau A, Lux-Steiner M, Jager-Waldau R, Burkhardt R and Bucher E 1990 *Thin Solid Films* **189** 339
[10] Pouzet J and Bernède J C 1990 *Rev. Phys. Appl.* **25** 907
[11] Ouadah A, Pouzet J and Bernède J C 1993 *J. Physique III* **3** 1
[12] Jager-Waldau A, Lux-Steiner M, Jager-Waldau G and Bucher E 1993 *Appl. Surf. Sci.* **70–1** 731
[13] Pawlikowski J M 1990 *Thin Solid Films* **190** 39
[14] Hofmann W K 1988 *J. Mater. Sci.* **23** 3981
[15] Chatzitheodorou G, Fiechter S, Kunst M, Luck J and Tributsch H 1988 *Mater. Res. Bull.* **23** 1261
[16] Maschke K and Levy F 1984 *Landolt–Bornstein New Series* Group III, vol 17F, ed O Madelung, M Schulz and H Weiss (Berlin: Springer) ch 9.7, pp 281–1316
[17] Zabinski J J, Donley M S, Prasad S V and McDevitt N T 1994 *J. Mater. Sci.* **29** 4834
[18] Tiefenbacher S, Sehnert H, Pettenkofer C and Jaegermann W 1994 *Surf. Sci.* **318** L1161
[19] Genut M, Margulis L, Hodes C and Tenne R 1992 *Thin Solid Films* **217** 91
[20] Genut M, Margulis L, Tenne R and Hodes C 1993 *Thin Solids films* **219** 30
[21] Benhida S, Bernède J C, Pouzet J and Barreau A 1993 *Thin Solid Films* **224** 39
[22] Bernède J C and Benhida S 1994 *J. Mater. Sci.* **29** 5972
[23] Mallouky A and Bernède J C 1988 *Thin Solid Films* **158** 285
[24] Wagner C D, Riggs W M, Davis L E, Moulder S F and Muilenberg G E 1979 *Handbook of X-ray Photoelectron Spectroscopy* (Eden Prairie, MN: Perkin–Elmer)
[25] Janda M and Kubovy A 1976 *Phys. Status Solidi* a **35** 391
[26] Beal A R, Liany W Y and Hughes H P 1976 *J. Phys. C: Solid State Phys.* **9** 2449
[27] Seto S Y 1975 *J. Appl. Phys.* **46** 5247
[28] Baccarini G, Ricco B and Spadini G 1978 *J. Appl. Phys.* **49** 5565

[29] Lu C C, Luan C Y and Meindl J D 1981 *IEEE Trans. Electron. Devices* **2F** 818
[30] Werner J H 1994 *Solid State Phenom.* **37–8** 213
[31] Werner J H and Guttler H H 1991 *J. Appl. Phys.* **69** 1522
[32] Bernède J C, Pouzet J, Le Ny R and Ben Nasrallah T 1994 *J. Physique III* **4** 677
[33] Khelil A, Essaidi H, Bernède J C, Bouacheria A and Pouzet J 1994 *J. Phys.: Condens. Matter* **6** 8527
[34] Fortin B, Mohammed-Brahim J, Mostefa D, Sarret M and Bonnaud O 1994 *Proc. 4ème Journées Maghrébines des Sciences des Matériaux (Casablanca 1994)* (:) p 101